Available online at www.sciencedirect.com
SCIENCE DIRECT®
ELSEVIER
Journal of Chromatography A, 989 (2003) 3–17
JOURNAL OF CHROMATOGRAPHY A
www.elsevier.com/locate/chroma

Comparison of preparative characteristics of micro open parallel plate separators and microbore columns for concentration of trace species by displacement chromatography

Blanca H. Lapizco-Encinas, Neville G. Pinto*

Department of Chemical Engineering, 696 Rhodes Hall, P.O. Box 210171, Cincinnati, OH 45221-0171, USA

Abstract

The potential for preparative concentration of trace species by displacement chromatography in a micro open parallel plate separator (μOPPS) has been explored. A comparison of the performance of the μOPPS with micro open tubular columns (μOTC) has been presented. Using simulation models, the effects of operating and equilibrium parameters on throughput and yield have been determined. It is shown that the μOPPS can offer considerable advantages over the traditional μOTCs. Most significantly, throughputs can be enhanced by more than an order of magnitude in many cases. This is primarily due to the higher loading per cycle in the μOPPS, made possible by the ability to change the depth of the channel independent of the width. While yield is generally lower in the μOPPS, this effect can be overcome by the proper selection of operating conditions.

Keywords: Micro open parallel plate separator; Preparative chromatography; Mathematical modelling; Column characterization; Displacement chromatography

1. Introduction

In preparative chromatography, the focus of a separation is on maximizing production rate and recovery. These objectives require operating the column under overloaded conditions [1–3]. Overloaded elution chromatography is widely used as a preparative purification process. Displacement chromatography has been suggested as an alternative, to exploit potential benefits such as the integration of concentration and purification in a single step, high column loading, and high throughput and purity with low solvent consumption [3–6]. In a displacement operation, the sample containing the product to be purified is loaded onto the chromatographic column, and is subsequently desorbed by a displacing agent whose thermodynamic affinity for the stationary phase is greater than that of the desired product. Ideally, the product is obtained as a rectangular band in a displacement train made up of the product, contaminants and the displacer. The process is described in detail elsewhere [7,8]. The use of displacement chromatography is, however, not as widespread as elution chromatography, though the technique has gained importance in separation of proteins and biomolecules [6,9–14], and methods that involve solute self-displacement have been studied [15], as well as selective displacement [16].

*Corresponding author. Tel.: +1-513-556-2761; fax: +1-513-556-3473.

E-mail address: neville.pinto@uc.edu (N.G. Pinto).

0021-9673/02/$ – see front matter
PII: S0021-9673(02)01609-6

The ability to fractionate a sample and simultaneously concentrate the fractionated species makes displacement chromatography particularly attractive for the enrichment of trace species. Preparative separations of trace components present a special challenge. Dilution due to column volume is a problem regardless of the mode of chromatographic development. Furthermore, in cases where the sample amount is limited or expensive, preparation on conventional bench-scale systems is impractical. Consequently, preparative separations of trace species are often performed on microbore columns. This approach offers gains in detection and sensitivity, as well as increased yield and concentration factors, with reduced solvent consumption and the possibility of easy coupling with other techniques [17–20]. The use of microbore columns does however raise some problems; column capacity is low, and carrier velocities are limited by the higher pressure-drop. Both factors adversely affect throughput.

Recently, the feasibility of using a micro open parallel plate separator (μOPPS) for chromatographic separations has been experimentally demonstrated [21]. It has been shown that the rectangular flow cross-section of the μOPPS offers significant advantages for analytical elution separations, including very low separation impedances and integrated detection [22]. The geometry of the μOPPS can also offer advantages for preparative separations of trace species. The additional flexibility in varying depth independent of width allows enhanced carrier velocities, relative to microbore columns, and increased active surface area per unit length. Additionally, when used with displacement development the combined effects of a microcolumn volume, higher surface capacity and carrier velocity can be expected to enhance product throughput.

The specific objective of this study was to explore the capabilities of the μOPPS to concentrate trace species in the displacement mode. A comparison of the preparative potential of the μOPPS and microbore columns, also known as micro open tubular columns (μOTC), has been made. Additionally, a parametric study has been performed to relate operating and equilibrium conditions to product throughput for the μOPPS.

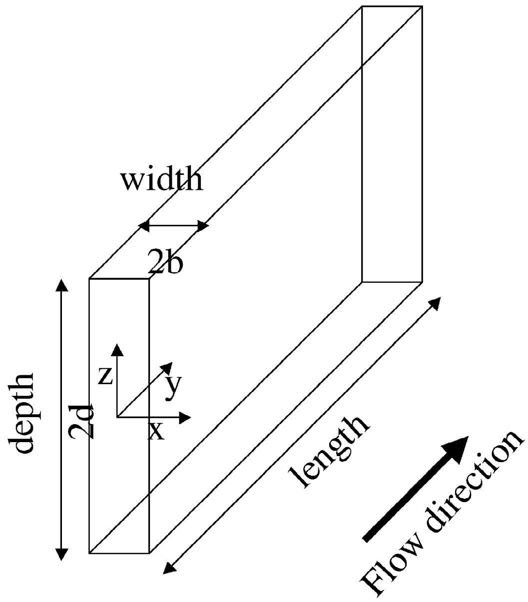

Fig. 1. Schematic representation of a μOPPS.

2. Theory

A schematic representation of the μOPPS is shown in Fig. 1. It is assumed that the flow regime in this channel is laminar and fully developed with negligible end effects. For this case, Spangler [23] has shown that the velocity profile is given by:

$$v_y = -3v_{\mathrm{avg}} \cdot \left(\frac{b^2+d^2}{b^2d^2}\right) \cdot \left(\frac{(x^2-b^2)(z^2-d^2)}{(x^2-b^2)+(z^2-d^2)}\right) \tag{1}$$

where v_y is the linear velocity in the fluid flow (length) direction, v_{avg} is the average linear velocity, b is half of microchannel width, d is half of microchannel depth, x and z are the positions along the microchannel width and depth, respectively.

Adsorption of the solute is assumed to take place on the surfaces defined by the depth and length dimensions (side surfaces) of the channel, while the surfaces defined by the width and the length (top and bottom surfaces) are assumed to be inactive. This choice is based on the experimental μOPPS developed earlier [21,24]; the top/bottom surfaces are inert, while the side surfaces are activated for ion-exchange. It is further assumed that the adsorption (or ion-exchange) step is instantaneous relative to the mass-transfer rate. The mass-transfer resistance is in the liquid phase, since the surface is assumed nonporous and ideally two-dimensional. Upon injection, the sample is assumed to be evenly distributed along the channel cross-section, and the fluid density is assumed constant. A pre-determined volume of the trace species is injected, and immediately followed by the displacer.

The Langmuir isotherm model for multiple components was selected to describe the equilibrium behavior:

$$q_i^* = \frac{Vm_i K_i C_i}{1 + \sum_{h=1}^{nc} K_h C_h} = \frac{a_i C_i}{1 + \sum_{h=1}^{nc} K_h C_h} \tag{2}$$

where: q_i^* is the equilibrium concentration of solute in the stationary phase, C_i is the solute concentration in the mobile phase, Vm_i is the adsorption capacity, K_i is the affinity toward the stationary phase, and a_i is the product of Vm_i and K_i.

With these assumptions, it can be shown that the continuity equation for a solute in the channel is:

$$\frac{\partial C_i}{\partial t} - 3\frac{\partial C_i}{\partial y}\cdot v_{\text{avg}}\cdot\left(\frac{b^2+d^2}{b^2 d^2}\right)\cdot\left(\frac{(x^2-b^2)(z^2-d^2)}{(x^2-b^2)+(z^2-d^2)}\right) = D_i\cdot\left(\frac{\partial^2 C_i}{\partial x^2} + \frac{\partial^2 C_i}{\partial y^2} + \frac{\partial^2 C_i}{\partial z^2}\right) \tag{3}$$

where: y is the position along the microchannel length and D_i is the diffusion coefficient of solute in the fluid.

For convenience the following dimensionless variables are defined:

Dimensionless time: $\tau = \dfrac{v_{\text{avg}} t}{L}$ $\quad \theta_{X,i} = \dfrac{v_{\text{avg}} b^2}{D_i L}$

$$\theta_{Z,i} = \frac{v_{\text{avg}} d^2}{D_i L} \tag{4}$$

Dimensionless spatial position: $X = \dfrac{x}{b}$ $\quad Y = \dfrac{y}{L}$

$$Z = \frac{z}{d} \tag{5}$$

Peclet number: $$Pe_i = \frac{v_{\text{avg}} L}{D_i} \tag{6}$$

where L is the length of the microchannel.

Re-writing Eq. (3) in terms of these parameters:

$$\frac{\partial C_i}{\partial \tau} - 3\cdot\frac{\partial C_i}{\partial Y}\cdot\left(\frac{b^2+d^2}{d^2}\right)\cdot\left(\frac{(X^2-1)\cdot(Z^2-1)}{\frac{b^2}{d^2}\cdot(X^2-1)+(Z^2-1)}\right) = \frac{1}{\theta_{X,i}}\cdot\frac{\partial^2 C_i}{\partial X^2} + \frac{1}{Pe_i}\cdot\frac{\partial^2 C_i}{\partial Y^2} + \frac{1}{\theta_{Z,i}}\cdot\frac{\partial^2 C}{\partial Z^2} \tag{7}$$

For displacement chromatography, with no solute present in the channel at the start of the separation, the following initial and boundary conditions apply:

Initial condition: At $\tau = 0$ $\quad C_i(X,Y,Z) = 0$

$$0 \le X \le 1,\ 0 \le Y \le 1,\ 0 \le Z \le 1 \tag{8}$$

2.1. Boundary conditions

At the channel walls (side surfaces), the solute diffusion flux in the liquid is equal to the accumulation at the surface due to adsorption:

$$\text{at } X = \pm 1 \quad -D_i\frac{\partial C_i}{\partial x}\bigg|_{x=b} = \frac{\partial q_i^*}{\partial t} \tag{9}$$

after substitution of the equilibrium condition (Eq. (2)), Eq. (9) becomes:

$$\frac{\partial C_i}{\partial X}\bigg|_{X=1} = -\frac{Vm_i K_i v_{\text{avg}}}{L}\cdot\frac{b}{D_i}\cdot\left(\frac{\left(1+\sum_{h=1}^{nc} K_h C_h\right)\frac{\partial C_i}{\partial \tau} - C^n_{k,MX,m,i}\sum_{h=1}^{nc} K_h\frac{\partial C_h}{\partial \tau}}{\left(1+\sum_{h=1}^{nc} K_h C_h\right)^2}\right) \tag{10}$$

It is usual to assume that there is no concentration gradient at the channel exit. Thus:

$$\text{at } Y = 1 \quad \frac{\partial C_i}{\partial Y}\bigg|_{Y=1} = 0 \tag{11}$$

Since the top and bottom cover plates of the μOPPS are assumed inert, there is no flux at these plates. Thus:

$$\text{at } Z = \pm 1 \quad -D_i \left.\frac{\partial C_i}{\partial Z}\right|_{Z=1} = 0 \tag{12}$$

from symmetry:

$$\text{at } X = 0, \quad \left.\frac{\partial C_i}{\partial X}\right|_{X=0} = 0 \tag{13}$$

and:

$$\text{at } Z = 0, \quad \left.\frac{\partial C_i}{\partial Z}\right|_{Z=0} = 0 \tag{14}$$

Finally, for the solute (component 1):

$$\text{at } Y = 0, \quad C_1(X,0,Z) = CF_1 \quad 0 \leq \tau \leq \tau_{F,1} \tag{15}$$

$$C_1(X,0,Z) = 0 \quad \tau > \tau_{F,1} \tag{16}$$

and, for the displacer (component 2):

$$\text{at } Y = 0, \quad C_2(X,0,Z) = CF_2 \quad \tau_{F,1} \leq \tau \leq \tau_{F,2} \tag{17}$$

$$C_1(X,0,Z) = 0 \quad \tau > \tau_{F,2} \tag{18}$$

where: τ_F is the dimensionless feed time and CF is the feed concentration.

In order to solve Eq. (7), the numerical method of finite differences was applied. Forward difference was used for the first-order time derivative and central difference for all the spatial derivatives. The alternating direction implicit scheme was employed to obtain a stable solution. This scheme divides each time interval between the number of spatial directions (in this case three directions): channel width, depth and length. Each spatial direction is represented by a tridiagonal matrix of equations, which is solved using the LU-decomposition method (tridiagonal matrix method).

The particular scheme used is the Peaceman–Rachford algorithm, which is described in detail elsewhere [25]. The numerical method uses four indices: n, j, k and m for time, width, length and depth, respectively. For convenience, the following finite difference terms are defined:

$$R_{X,i} = \frac{\Delta\tau}{\theta_{X,i}\Delta X^2} \quad R_{Y,i} = \frac{\Delta\tau}{Pe_i \Delta Y^2}$$

$$R_{Z,i} = \frac{\Delta\tau}{\theta_{Z,i}\Delta Z^2} \quad S_Y = -\frac{3\,\Delta\tau}{2\,\Delta Y} \cdot \left(\frac{b^2}{d^2} + 1\right)$$

$$\delta_X^2 C_{j,k,m,i}^n = C_{j-1,k,m,i}^n - 2C_{j,k,m,i}^n + C_{j+1,k.m,i}^n$$

$$\delta_Y^2 C_{j,k,m,i}^n = C_{j,k-1,m,i}^n - 2C_{j,k,m,i}^n + C_{j,k+1,m,i}^n$$

$$\delta_Z^2 C_{j,k,m,i}^n = C_{j,k,m-1,i}^n - 2C_{j,k,m,i}^n + C_{j,k,m+1,i}^n$$

$$\delta_{Y0} C_{j,k,m,i}^n = C_{j,k-1,m,i}^n - C_{j,k+1,m,i}^n$$

Substituting in Eq. (7):

$$C_{j,k,m,i}^{n+1} - C_{j,k,m,i}^n + \delta_{Y0} C_{j,k,m,i}^n S_Y \cdot \left(\frac{(X_j^2 - 1)\cdot(Z_m^2 - 1)}{\frac{b^2}{d^2}(X_j^2 - 1) + (Z_m^2 - 1)}\right) = R_{X,i}\delta_X^2 C_{j,k,m,i}^n + R_{Y,i}\delta_Y^2 C_{j,k,m,i}^n + R_{Z,i}\delta_Z^2 C_{j,k,m,i}^n \tag{19}$$

Eq. (19) was broken into three parts, and each part generated a system of equations, which were solved in separate numerical subroutines. An additional parameter was used to describe the depth to width ratio:

$$\alpha = \frac{\theta_Z}{\theta_X} = \left(\frac{d}{b}\right)^2 \tag{20}$$

Throughput (TH) was calculated as follows:

$$TH = \frac{m_S}{T_{FT} + T_D} \tag{21}$$

where: m_S is the mass trace species product, T_{FT} is the total feed time for both trace species and the displacer, and T_D is defined as the time required to elute the displacer from the column; T_D therefore includes the regeneration time. Only product with a specified purity (99%) and with a concentration higher than the feed ($C > CF$) was accounted for in the TH. The percentage yield was evaluated as follows:

$$\text{Yield} = \frac{m_S}{m_{ST}} \cdot 100\% \tag{22}$$

where m_{ST} is the total mass of solute introduced into the μOPPS.

The pressure drop across the μOPPS was calculated from [26]:

$$\Delta P = \frac{3\mu L v_{\mathrm{avg}}}{b^2} \tag{23}$$

where μ is the mobile phase viscosity.

In order to compare the preparative characteristics of the μOPPS with a microbore (μOTC) column, the μOTC was simulated using the following equation:

$$\frac{\partial C_i}{\partial \tau} + 2(1-R^2)\cdot\frac{\partial C_i}{\partial Y} = \frac{1}{Pe_i}\cdot\frac{\partial^2 C_i}{\partial Y^2} + \frac{1}{\theta_{R,i}}\cdot\frac{1}{R}\cdot\frac{\partial C_i}{\partial R} + \frac{1}{\theta_{R,i}}\cdot\frac{\partial^2 C_i}{\partial R^2} \tag{24}$$

R is the dimensionless radius of the column, and $\theta_{R,i}$ is defined as:

$$\theta_{R,i} = \frac{v_{\mathrm{avg}} r_C^2}{D_i L} \tag{25}$$

where r_C is the radius of the μOTC. Eq. (24) was solved using a numerical procedure analogous to that used for Eq. (7).

The pressure drop of the μOTC was calculated from [26]:

$$\Delta P = \frac{8\mu L v_{\mathrm{avg}}}{r_C^2} \tag{26}$$

3. Results and discussion

The comparisons of performance of the μOPPS and the μOTC for concentrating trace species were made using the simulation parameters shown in Table 1, unless otherwise stated. The trace species was assumed to be KBr exchanging on a polyethyleneimine (PEI) activated surface, to enable characteristics to be estimated from data in the literature [21,27]. The radius (r_C) of the μOTC was kept equal to the half width (b) of the μOPPS for all the comparisons. The lengths of the two separators were kept the same, and the value selected corresponds to the channel length in the prototype μOPPS developed earlier [21,24].

Shown in Fig. 2 are typical effluent concentration histories for the μOPPS and μOTC obtained from the simulations. Results such as these were used to make comparisons of performance between the systems. Shown in Fig. 3 is the relative throughput predicted as a function of the Peclet number (Pe). Since the length and diffusivity have been kept constant throughout (Table 1), an increase in Pe corresponds to an increase in linear velocity v_{avg}. The throughput ratios calculated are for a product purity of 99%. Also shown in Fig. 3 is the effect of α on throughput; this ratio was changed by changing the depth of the channel while keeping the width constant and equal to the diameter of the μOTC ($\theta_R = \theta_X$). Clearly, there is a significant advantage gained by using the μOPPS configuration. For the systems studied, at $Pe < 4.5\cdot 10^4$ a throughput between 2 and 7 times larger can be achieved. This is due to a combination of factors. First, the μOPPS has a larger volume than the μOTC in all cases, and since the systems are volume overloaded (1.2 VC), the amount loaded per cycle is larger on the μOPPS; this effect becomes stronger as α is increased. Secondly, due to the smaller active surface area in the μOPPS, the retention times for the displacer and regeneration fronts are shorter, which directly influences throughput (Eq. (21)).

The decrease in the throughput ratio with increasing Pe can be explained as follows. As Pe increases, the concentration wave velocity in the flow direction

Table 1
Simulation parameters used for the comparison between μOPPS and μOTC

Equilibrium and kinetic parameters		
K_1 ($\mathrm{cm^3/\mu mol}$)	79.2	
K_2 ($\mathrm{cm^3/\mu mol}$)	316.8	
Vm_1 ($\mathrm{\mu mol/cm^2}$)	$1.0\cdot 10^{-4}$	
Vm_2 ($\mathrm{\mu mol/cm^2}$)	$7.2\cdot 10^{-5}$	
D_1 ($\mathrm{cm^2/s}$)	$2.0\cdot 10^{-5}$	
D_2 ($\mathrm{cm^2/s}$)	$2.0\cdot 10^{-5}$	
Operating parameters	μOPPS	μOTC
L (cm)	3.00	3.00
b (μm)	25.00	
r_C (μm)		25.00
CF_1 ($\mathrm{\mu mol/cm^3}$)	0.01	0.01
CF_2 ($\mathrm{\mu mol/cm^3}$)	0.10	0.10
VF_1 (VC)	1.20	1.20
VF_2 (VC)	0.50	0.50

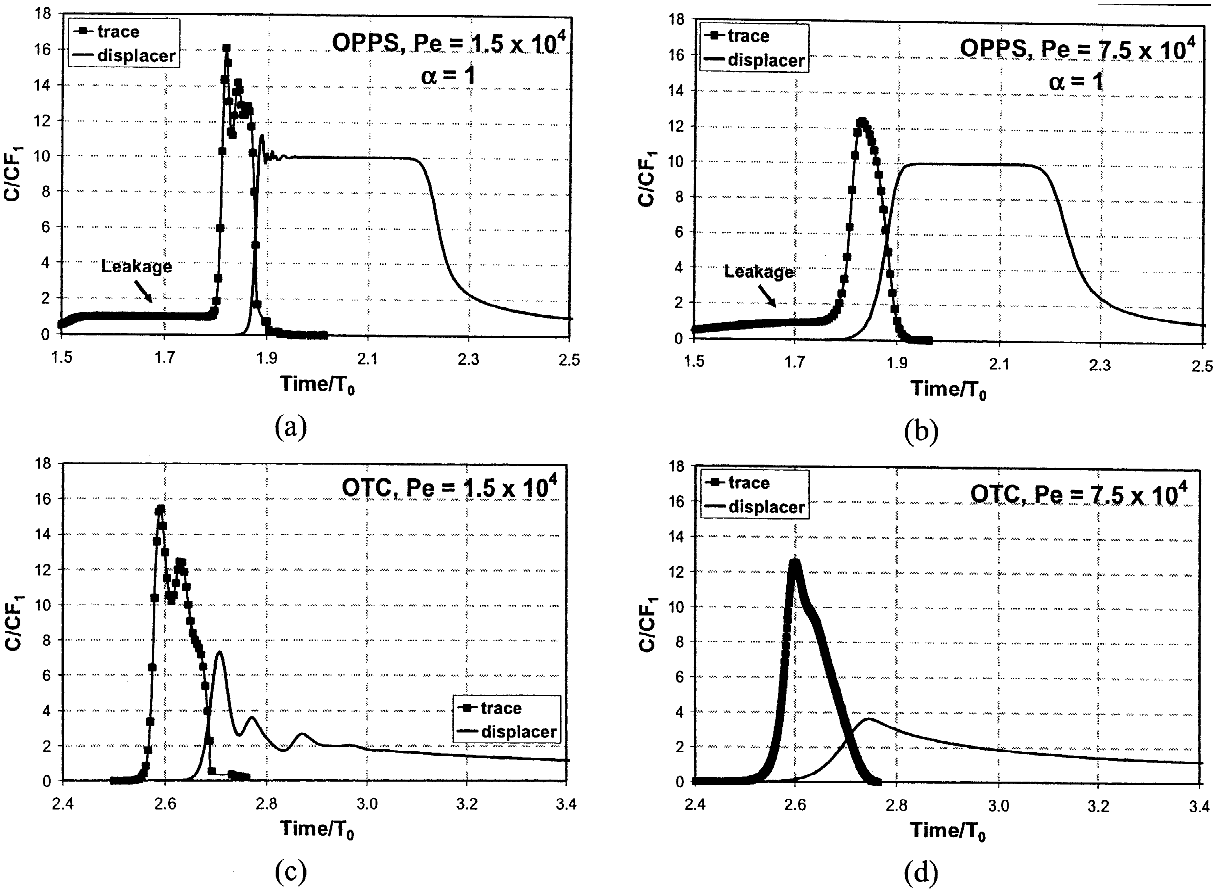

Fig. 2. Chromatographic peaks obtained from simulations for μOPPS and μOTC as a function of *Pe*.

increases reducing the total time per cycle. However, the time constant for diffusive flow toward the adsorptive surface does not change. The consequence for both μOPPS and μOTC is that the throughput decreases, due to reduced mass transfer to the wall. It is important to note that, due to the lower retention in the μOPPS, increasing *Pe* can have a much stronger effect on performance for this channel geometry. For example, in Fig. 3, the throughput of the μOPPS is shown to drop to one tenth that of the μOTC at very high values of *Pe*.

Fig. 4 shows the yield, at 99% purity, corresponding to the throughputs in Fig. 3. For the μOPPS, the yield depends on α for values of α close to 1, and is essentially independent of α at higher values. The yield of the μOTC is always greater than the yield of the μOPPS. For both separators the yield drops as the *Pe* is increased, but the effect is stronger for the μOPPS, for the reason explained above, and this results in a lower yield ratio with increasing *Pe*.

The performance of the μOPPS is very sensitive to the width of the channel. This is illustrated in Fig. 5. These results were obtained at a *Pe* of $3 \cdot 10^4$ and $\alpha = 16$, and are reported as a function of $\theta_{X,}$ which is directly related to the microchannel width (Eq. (4)); it is important to mention that in order to keep *Pe* and α constant, *b*, *d* and θ_Z were varied. Clearly, the performance in terms of both throughput and yield is a very strong function of the diffusion path length in the width direction. In particular, at small θ_X both throughput and yield fall rapidly for small increases in θ_{X}.. This is due to a rapid weakening of the displacement effect due to product leakage and increased overlapping of zones as the width is

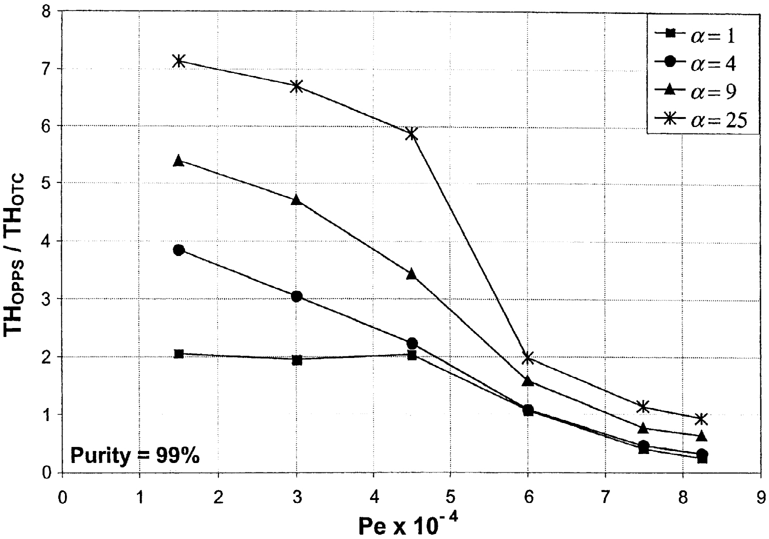

Fig. 3. Relative throughput at 99% purity as function of *Pe* and α.

increased. These features are apparent in the chromatograms shown in Fig. 6.

The results in Fig. 5 suggest it should be possible to overcome the sensitivity of the throughput and yield of the μOPPS to *Pe* (Figs. 3 and 4) by narrowing the channel. Shown in Figs. 7 and 8 are the throughput and yield curves as a function of *Pe* for 10 μm half width (*b*) or radius (r_C). The throughput advantage of the μOPPS is significantly enhanced as the flow channel is narrowed. Comparing Figs. 7 and 3, the relative throughput in all cases more than doubles, for a decrease in the half-width/radius from 25 to 10 μm. Also, very significantly, the throughput ratio is relatively insensitive to the *Pe* at 10 μm, and the μOPPS is predicted to give much higher throughputs even at very high values of *Pe*. A

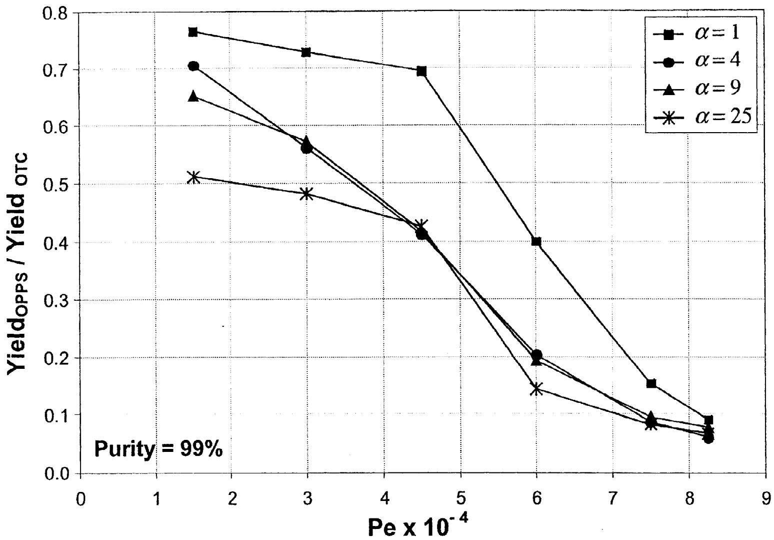

Fig. 4. Relative yield at 99% purity as function of *Pe* and α.

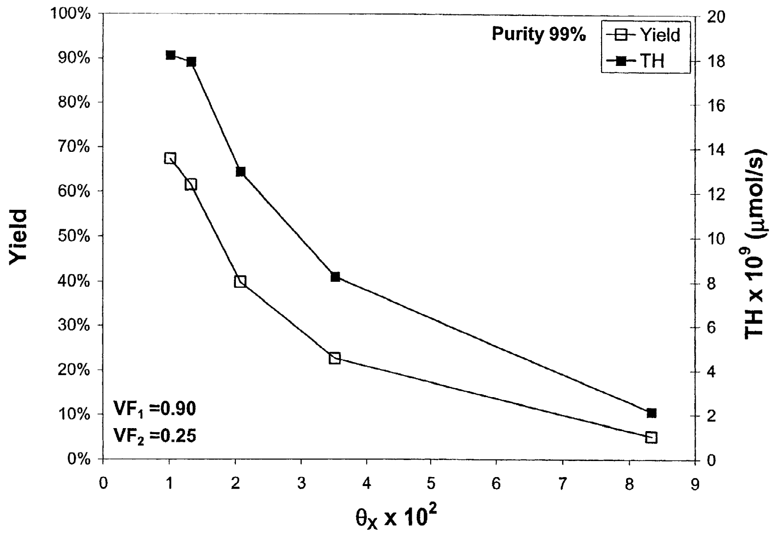

Fig. 5. Throughput and yield obtained from simulations for μOPPS as function of θ_X.

narrower channel also improves the relative yield considerably. For the entire range of *Pe* studied, the 10 μm half-width μOPPS gives yields that are between 75 and 95% of the yield of the μOTC (Fig. 8). This is a significant improvement over the 25-μm case (Fig. 4).

An added advantage of the μOPPS is the lower pressure drop exerted by this geometry. All the comparisons of throughput shown so far have been at identical *Pe*, which in effect means the same carrier velocity, since the length and diffusivity are constant. However, at identical carrier velocities, the pressure drops in the μOPPS and μOTC are different. Even with $\alpha = 1$, the pressure drop in the μOPPS is considerably lower than the equivalent $(\theta_R = \theta_X)$ μOTC. This is clearly seen in Fig. 9, where the differences are compared at two $\theta_X = \theta_R$ values. The advantage of μOPPS is particularly significant for the narrower geometries, which are desirable for maximizing throughput and yield.

The effects of the feed concentration of the trace species (CF_1) were also studied, and are shown in Fig. 10. At very low feed concentrations of solute, both separators are inefficient because column conditions are in the linear region of the isotherm and there is no displacement. The μOPPS needs a higher loading than the μOTC to be in the non-linear region. Therefore, under extreme conditions ($CF_1 < 5.0 \cdot 10^{-3}$) the performance of the μOPPS is substantially inferior to the performance of the μOTC.

However, when displacement of the trace does occur, the μOPPS gives a higher throughput and the μOTC gives a higher yield. A weak minimum is present in both the relative throughput and relative yield curves. In general, the relative throughput and yield increase with increasing feed concentration until the influence of leakage in the μOPPS becomes significant. For the conditions in Fig. 10, this occurs $CF_1 = 0.01$ μmol/cm^3. At higher feed concentrations the relative throughput and yield decrease until the effects of leakage are equally significant in the μOTC.

The results in Fig. 10 and all subsequent figures are for a half-width/radius of 25 μm; this was done to reduce computational time. It is important to remember, as was shown earlier, that throughput, relative throughput, yield and relative yield can all be increased by decreasing the half-width/radius.

Fig. 11 shows the effect of the feed volume of solute (VF_1) on relative performance. The throughput and yield ratios increase to a maximum ($VF_1 = VC$) and then decrease at higher volume loadings, similar to the trend seen with CF_1. The initial increase is due to the larger loading possible in the μOPPS. Beyond the maximum, the loss from leakage is more significant for the μOPPS, and the throughput and yield

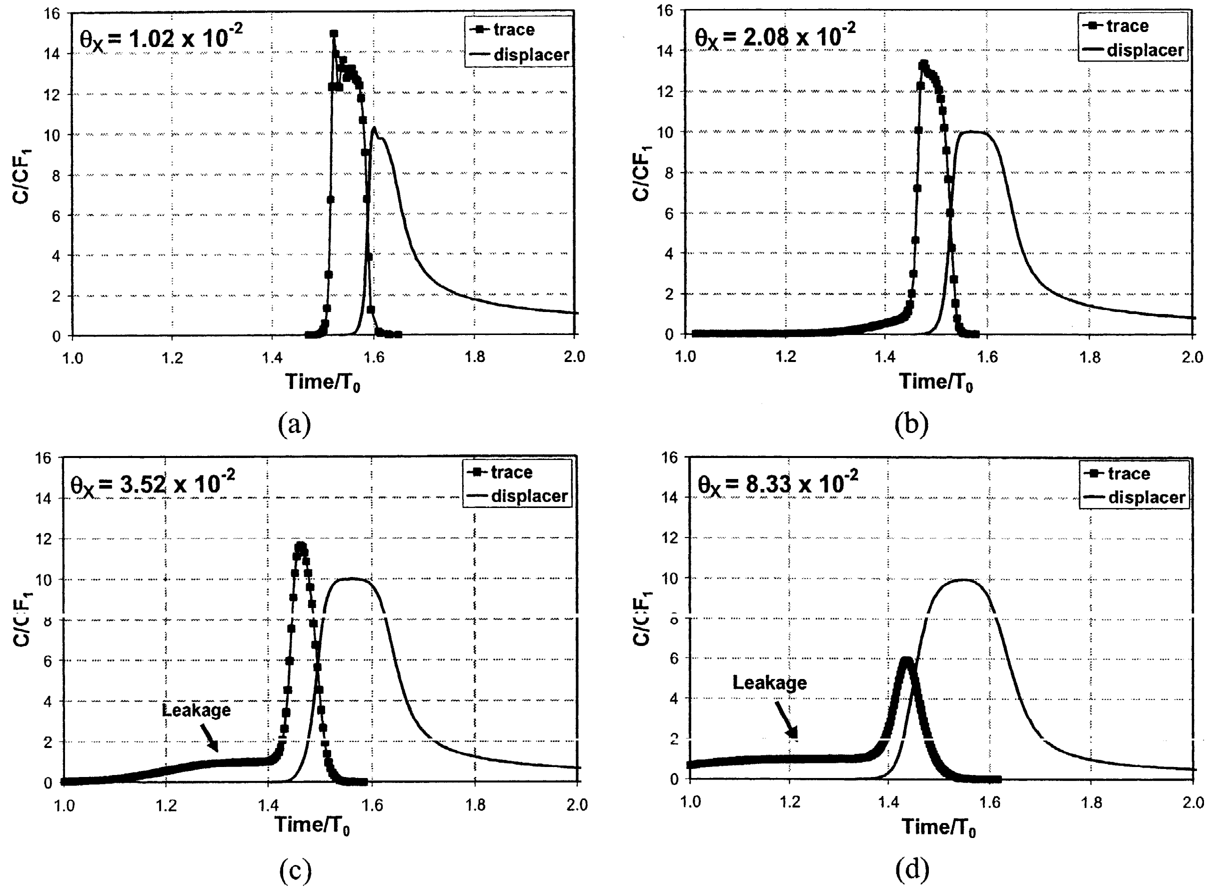

Fig. 6. Chromatographic peaks obtained from simulations for μOPPS as a function of θ_X.

ratios decrease. It is worth noting, however, that for the entire range of VF_1/VC where displacement occurs the μOPPS gives higher throughputs.

The effects of displacer concentration (CF_2) on the relative performance is shown in Fig. 12. At identical displacer concentrations, the μOPPS always gives a higher throughput. In general, the relative performance is independent of the displacer concentration above a certain concentration ($>65\cdot10^{-3}$ μmol/cm^3 in Fig. 12). When high concentrations of displacer are used, the performance of the μOPPS in terms of yield is much lower than the performance of the μOTC. An excess of displacer is detrimental to the performance of both systems, but it affects the μOPPS more strongly due to the lower retention in the μOPPS. Very significantly, however, at lower concentrations (<50 μmol/cm^3 in Fig. 12), it is shown that the μOPPS can simultaneously give higher throughputs and yields. At low displacer concentrations, the longer retention time in the μOTC can lead to sufficient dilution of the displacer to make it ineffective for displacement, resulting in poor product throughput. Low concentrations of displacer are generally desirable. Most obviously, they reduce the quantity of displacer required. Also, a lower loading of displacer per cycle reduces the volume of regenerant and time for regeneration. This can lead to a higher overall throughput. For example for the case illustrated in Fig. 12, the highest absolute throughput (distinct from the relative value) in the μOPPS is obtained at the low displacer concentration of 20 μmol/cm^3. This result clearly

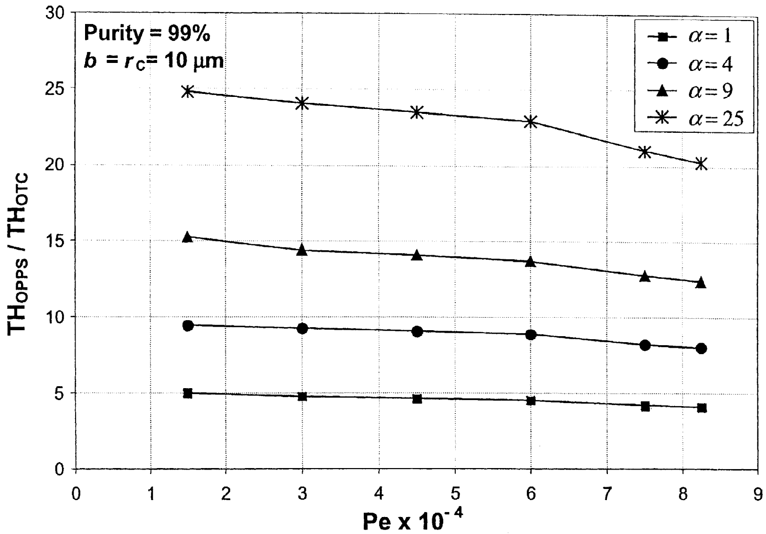

Fig. 7. Relative throughput at 99% purity as function of Pe and α; half width = 10 μm.

illustrates that with the proper selection of conditions higher throughputs can be realized in the μOPPS without necessarily incurring a lower yield.

The volume of displacer (VF_2) has a similar effect on the relative throughput and yield, as shown in Fig. 13. At low displacer volumes, dilution in the μOTC makes the displacer ineffective for displacement. Under these conditions, the μOPPS can simultan-

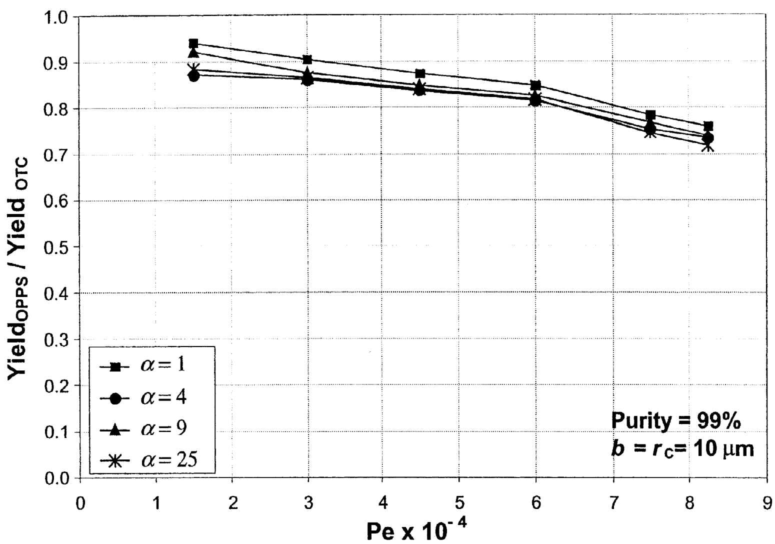

Fig. 8. Yield at 99% purity as function of Pe and α; half width = 10 μm.

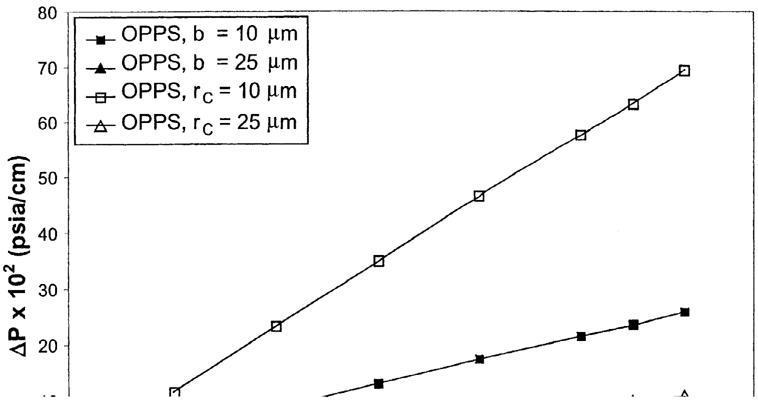

Fig. 9. ΔP as a function of *Pe*.

eously give higher throughputs and yields. As the displacer volume is increased the relative throughput and yield drops, and above a certain value the relative performance is insensitive to the volume of the displacer injected.

The influences of the Langmuir equilibrium parameters on the relative performance were also studied. Fig. 14 shows the influence of the ratio of the intrinsic capacity parameters, Vm_1/Vm_2, and Fig. 15 shows the influence of the ratio of the affinity

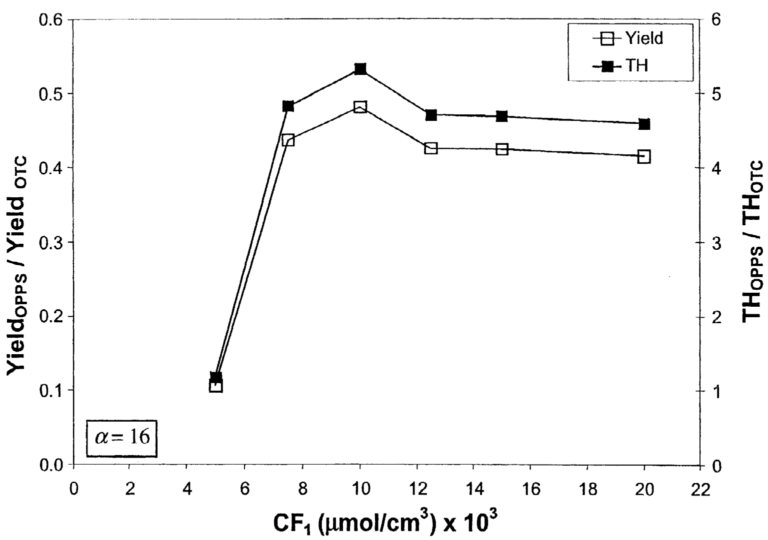

Fig. 10. Relative throughput and yield as a function of CF_1.

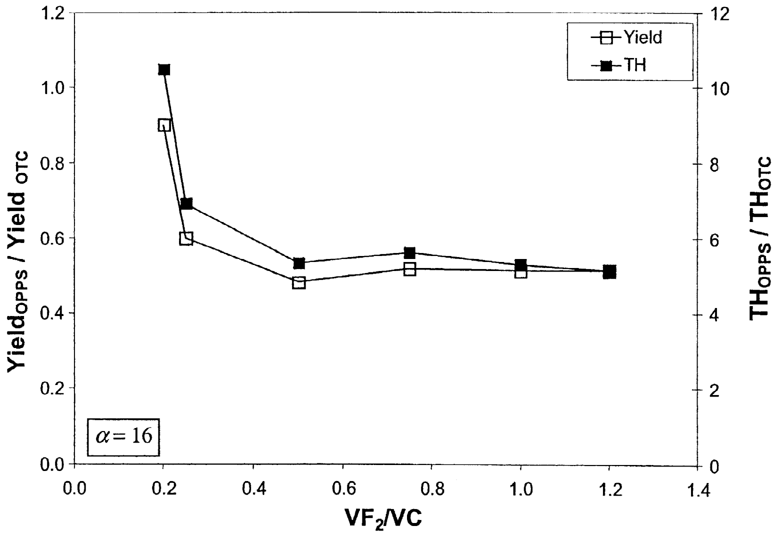

Fig. 13. Relative throughput and yield as a function of VF_2.

4. Conclusions

It is clear that a significant advantage can be gained by using the μOPPS in place of μOTC for preparative separations of trace components with displacement chromatography. Because of the ability to change the flow cross-section without significantly affecting mass-transfer efficiency, conditions can be selected to obtain throughputs that are significantly higher than in the μOTC. Although yields are generally lower in the μOPPS, narrower channels and the proper selection of displacer concentration

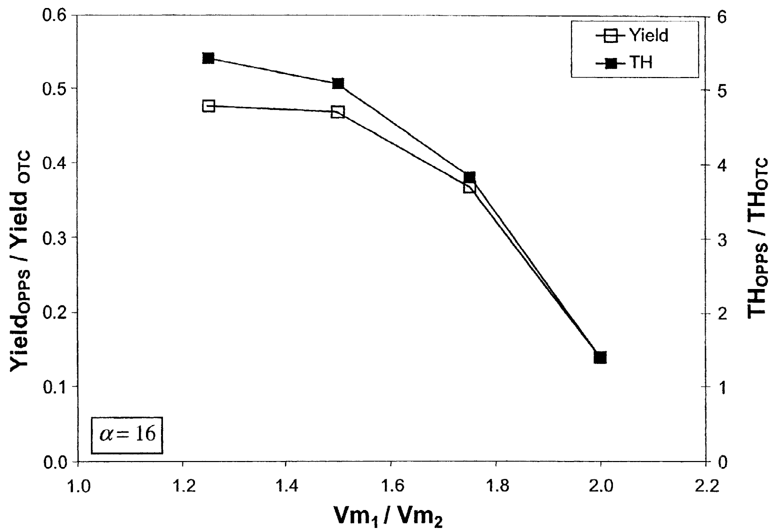

Fig. 14. Relative throughput and yield as a function of Vm_1/Vm_2.

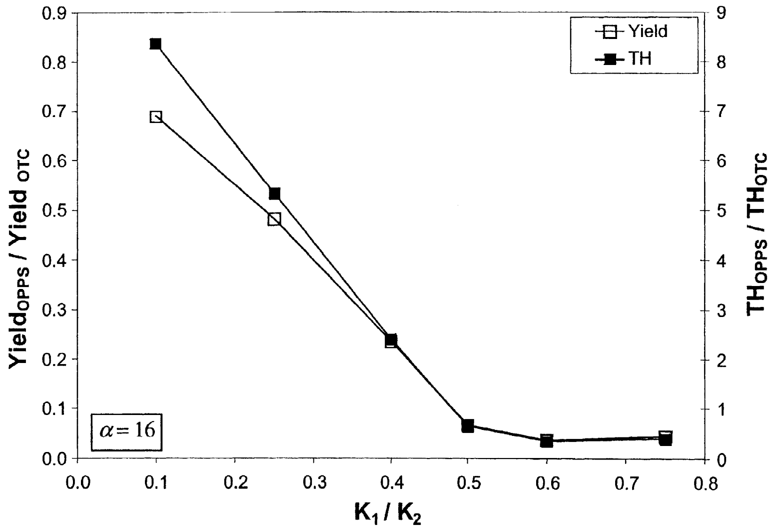

Fig. 15. Relative throughput and yield as a function of K_1/K_2.

and volume can be used to overcome the yield advantage of the μOTC while simultaneously maintaining the high throughput potential of the μOPPS.

5. Nomenclature

a	linear isotherm coefficient (cm), Eq. (2)
b	microchannel half width (cm)
C	solute concentration in the mobile phase (μmol/cm^3)
CF	feed concentration (μmol/cm^3)
d	microchannel half depth (cm)
D	diffusion coefficient in solution (cm^2/s)
K	Langmuir parameter (cm^3/μmol), used in Eq. (2)
L	microchannel length (cm)
m_S	mass of trace species product (μmol)
m_{ST}	total mass of trace species product (μmol)
Pe	Peclet number (dimensionless)
q^*	equilibrium concentration of solute in the stationary phase (μmol/cm^2), Eq. (2)
R	dimensionless radius
r_C	microcolumn radius (cm)
t	time (s)
T_D	displacer time, time that takes for the displacer to be eluted (s)
T_{FT}	total feed time (solute+displacer) (s)
TH	throughput (μmol/s), Eq. (21)
v_{avg}	average linear velocity along the length (cm/s)
VC	column volume (cm^3)
VF	feed volume (cm^3)
Vm	Langmuir parameter (μmol/cm^2), Eq. (2)
v_y	linear velocity along the length (cm/s)
X	dimensionless position along the microchannel width
x	position along the microchannel width (cm)
Y	dimensionless position along the microchannel length
y	position along the microchannel length (cm)
Z	dimensionless position along the microchannel depth
z	position along the microchannel depth (cm)

Greek symbols

ΔP	pressure drop (p.s.i.a.; 1 p.s.i. = 6894.76 Pa)
α	θ_Z/θ_X ratio (dimensionless)

μ	mobile phase viscosity (cP)
θ_R	dimensionless time (Eq. (25))
θ_X	dimensionless time (Eq. (4))
θ_Z	dimensionless time (Eq. (4))
τ	dimensionless time (Eq. (4))
τ_F	dimensionless feed time

Subsripts

i	component number, $1=$solute, $2=$ displacer

References

[1] P. Jandera, D. Komers, G. Guiochon, J. Chromatogr. A 796 (1998) 115.
[2] E.A. Staffan, R.K. Edvisson, Comput. Chem. Eng. 20 (1996) 507.
[3] S.C.D. Jen, N.G. Pinto, J. Chromatogr. 590 (1992) 3.
[4] A. Felinger, G. Guiochon, J. Chromatogr. A 796 (1998) 59.
[5] A. Kundu, S. Vunnum, S.M. Cramer, Adsorption 4 (1998) 373.
[6] A.A. Shukla, R.R. Deshmukh, J.A. Moore, S.M. Cramer, Biotechnol. Prog. 16 (2000) 1064.
[7] J. Frenz, Cs. Horváth, in: Cs. Horváth (Ed.), High-Performance Liquid Chromatography, Vol. 5, Academic Press, San Diego, CA, 1988, p. 212.
[8] G. Guiochon, S.G. Shirazi, A.M. Katti, Fundamentals of Preparative and Nonlinear Chromatography, Academic Press, Boston, MA, 1994.
[9] A. Kundu, S. Vunnum, S.M. Cramer, J. Chromatogr. A 707 (1995) 57.
[10] N. Tugcu, R.R. Deshmukh, Y.S. Sanghvi, J.A. Moore, S.M. Cramer, J. Chromatogr. A 923 (2001) 65.
[11] A.A. Shukla, R.L. Hopfer, D.N. Chakravarti, E. Bortell, S.M. Cramer, Biotechnol. Prog. 14 (1998) 92.
[12] R.S. Gallant, S.M. Cramer, J. Chromatogr. A 771 (1997) 9.
[13] G. Jayaraman, Y.F. Li, J.A. Moore, S.M. Cramer, J. Chromatogr. A 702 (1995) 143.
[14] Y.J. Kim, S.M. Cramer, J. Chromatogr. A 686 (1994) 193.
[15] J. Newburguer, B. DeLange, G. Guiochon, J. Chromatogr. A 684 (1994) 1.
[16] A. Kundu, K.A. Barnthouse, S.M. Cramer, Biotechnol. Bioeng. 56 (1997) 119.
[17] C. Southan, P. Lavery, K.G.M. Fantom, Anal. Biochem. 271 (1999) 152.
[18] D.B. Gomis, J.J. Mangas, A. Castaño, M.D. Gutiérrez, Anal. Chem. 68 (1996) 3867.
[19] Z. Wu, W.G. Tong, J. Chromatogr. A 805 (1998) 63.
[20] M.J. Mills, J. Maltas, W.J. Lough, J. Chromatogr. A 759 (1997) 1.
[21] Q. Kang, N.C. Golubovic, N.G. Pinto, H.T. Henderson, Chem. Eng. Sci. 56 (2001) 3409.
[22] B.H. Lapizco-Encinas, N.G. Pinto, Sep. Sci. Technol. 37 (2002) 2745.
[23] G. Spangler, Anal. Chem. 70 (1998) 4805.
[24] H.T. Henderson, N. deGouvea-Pinto, Liquid chromatograph on a chip, US Pat. 6258263B1 (2001).
[25] J.W. Thomas, Numerical Partial Differential Equations: Finite Difference Methods, Springer, New York, 1995.
[26] J.C. Giddings, J.P. Chang, M.N. Myers, J.M. Davis, K.D. Caldwell, J. Chromatogr. 255 (1983) 359.
[27] R.A. Robinson, D.H. Stokes, Electrolyte Solutions, 2nd ed, Butterworths, London, 1970.